Splitting of the 2^+ mixed symmetry mode in the proximity of the $N = 82$ shell closure

N. Lo Iudice,[1,*] Ch. Stoyanov,[2,†] and N. Pietralla[3,‡]

[1]*Dipartimento di Scienze Fisiche, Universitá di Napoli Federico II, and Istituto Nazionale di Fisica Nucleare, Monte S Angelo, Via Cintia, I-80126 Napoli, Italy*

[2]*Institute for Nuclear Research and Nuclear Energy, Bulgarian Academy of Sciences, 1784 Sofia, Bulgaria*

[3]*Institut für Kernphysik, Universität Darmstadt, D-64289 Darmstadt, Germany*

(Received 28 May 2009; published 21 August 2009)

The mixed symmetry 2^+ states in the $N = 84$ isotones ^{142}Ce and ^{144}Nd are investigated within the quasiparticle-phonon model, with special attention to their $M1$ decay to the lowest symmetric 2^+ state. The observed pronounced splitting of the $M1$ strength is shown to be caused by the phonon coupling, made quite effective by the peculiar shell structure of the two-valence neutrons above the $N = 82$ shell closure.

DOI: 10.1103/PhysRevC.80.024311 PACS number(s): 23.20.−g, 27.60.+j, 21.60.Ev

I. INTRODUCTION

Low-lying isovector excitations in open shell nuclei represent a unique laboratory for studying neutron-proton (np) correlations. In the np interacting boson model (IBM-2) [1], these excitations are described as mixed symmetry (MS) states with F spin $F = F_{\max} - 1$ [2–4]. The scissors mode [5,6], observed systematically in deformed nuclei [7–9], is the best known example of isovector or MS low-lying excitations.

MS states in spherical nuclei were searched for for a long time with partial success [10,11]. The search culminated, a decade ago, in an experiment on ^{94}Mo [12] that produced a large body of data about these states and their properties. A series of experiments has followed since then. They were devoted to ^{94}Mo [13–16] and to many other nuclei near the neutron magic number $N = 50$ [17–25]. The wealth of levels and transition probabilities produced by these experiments have greatly enriched the information about low-lying spectra in that region [26].

The measured spectra fit nicely within the IBM-2 theoretical framework. Indeed, they can be grouped into two main classes, one composed of symmetric states with maximum F spin ($F = F_{\max}$) and the other including the MS excitations with $F = F_{\max} - 1$. The states with the same F spin differing by one d boson are coupled by strong $E2$ transitions, those with the same number of d bosons and different F spins are connected by strong $M1$ transitions.

The IBM-2 level scheme and selection rules are confirmed by the microscopic quasiparticle-phonon model (QPM) [27–30], where the levels are classified according to the number of RPA phonons. The QPM gives insights also into the microscopic structure of these states and accounts for contributions coming from spin-flip excitations not considered in the IBM. Because of the large configuration space, the QPM is quite adequate for the description of collective phenomena. An alternative powerful approach is a shell model if the configuration space is sufficiently large. Indeed, several large-scale shell-model calculations have been attempted to explain the structure of MS states [11,18,31,32].

The full consistency with the IBM scheme proves the collective character of the observed low-lying levels, which is surprising in many respects. In general, at low energy, the shell structure and the spin degree of freedom play an important role. Therefore, one should have expected a pronounced damping and fragmentation of the, mainly orbital, $M1$ strength. This, instead, remains concentrated in a few select low-lying states.

To ascertain if this remarkable and, in many ways, unexpected property is peculiar to nuclei in the proximity of $N = 50$ or is a general feature, common to all nuclei in the proximity of shell closures, experimentalists have shifted their attention to the region around the $N = 82$ neutron shell closure.

Experiments on the $N = 80$ isotones [33–35] confirm the overall scheme obtained for the nuclei around $N = 50$. Some intriguing shell effects appear, nonetheless. The $M1$ strength in the $N = 80$ nuclide ^{138}Ce is not concentrated into a single transition connecting the MS $2^+_{\rm MS}$ to the corresponding symmetric 2^+_S but splits into two close peaks. No splitting is observed in the $N = 80$ isotone ^{136}Ba.

This picture is rendered even more contradictory by the results of earlier experiments on the $N = 84$ nuclides ^{142}Ce and ^{144}Nd [36,37]. In these isotones, in fact, the $M1$ strength associated with the MS mode splits into two prominent peaks much more widely separated than in ^{138}Ce.

A QPM investigation [38] has related the small $M1$ splitting in ^{138}Ce to the filling of the proton $1g_{7/2}$ subshell closure in correspondence with $Z = 58$. Because of the gap with the other subshells, the low-lying proton excitations are made possible only because of the diffuse Fermi surface induced by pairing. Several closely packed two-quasiparticle states appear at low energy with consequent increment of low-lying states of MS character, hence the fragmentation of the $M1$ strength. This is not the case for ^{136}Ba, where pairing plays a less important role in the excitation mechanism.

It is then natural to ask ourselves why the $M1$ splitting is more pronounced in ^{142}Ce, which has the same proton number as ^{138}Ce, and is equally large in ^{144}Nd, which has two more protons. Because ^{142}Ce and ^{144}Nd have the same neutron number, it is tempting to relate the alike $M1$ responses in these

*loiudice@na.infn.it
†stoyanov@inrne.bas.bg
‡pietralla@ikp.tu-darmstadt.de

two nuclei to the two-valence neutrons in excess with respect to the $N = 82$ shell closure.

Here we refine and expand a previous QPM study [39] to investigate in detail the 2^+ level schemes observed in the mentioned nuclei and attempt to clarify how the shell structure determines different $M1$ properties in different nuclei near the $N = 82$ shell closure.

II. A SKETCH OF THE QPM

The QPM [40] adopts a Hamiltonian composed of a Woods-Saxon one-body piece and a sum of several particle-particle and particle-hole multipole-multipole potentials.

The first step of the QPM procedure consists of expressing the Hamiltonian in terms of Bogoliubov quasiparticle creation and annihilation operators $\alpha^\dagger_{jm}$ and α_{jm}, respectively.

The quasiparticle separable Hamiltonian so obtained is then adopted to generate the QRPA energies $\omega_{i\lambda}$ and the corresponding phonons,

$$Q^\dagger_{i\lambda\mu} = \frac{1}{2}\sum_{jj'}\left\{\psi^{i\lambda}_{jj'}[\alpha^\dagger_j\alpha^\dagger_{j'}]_{\lambda\mu} - (-1)^{\lambda-\mu}\varphi^{i\lambda}_{jj'}[\alpha_{j'}\alpha_j]_{\lambda-\mu}\right\}. \tag{1}$$

The $\psi^{i\lambda}_{jj'}$ and $\varphi^{i\lambda}_{jj'}$ amplitudes fulfill the equation

$$\frac{1}{2}\sum_{jj'}\left[\psi^{i\lambda}_{jj'}\psi^{i'\lambda}_{jj'} - \varphi^{i\lambda}_{jj'}\varphi^{i'\lambda'}_{jj'}\right] = \delta_{ii'}\delta_{\lambda\lambda'}, \tag{2}$$

obtained from enforcing the normalization condition

$$\begin{aligned}\langle 0|Q_{i'\lambda'\mu'}Q^\dagger_{i\lambda\mu}|0\rangle &= \langle 0|[Q_{i'\lambda'\mu'}, Q^\dagger_{i\lambda\mu}]|0\rangle \\ &\simeq \delta_{ii'}\delta_{\lambda\lambda'}\delta_{\mu\mu'},\end{aligned} \tag{3}$$

valid in the quasiboson approximation. Once the QRPA phonons are generated, it is possible to express the quasiparticle separable Hamiltonian in the phonon form

$$H_{\rm QPM} = \sum_{i\mu}\omega_{i\lambda}Q^\dagger_{i\lambda\mu}Q_{i\lambda\mu} + H_{vq}, \tag{4}$$

where the first term is the unperturbed phonon Hamiltonian and H_{vq} is a phonon-coupling piece whose exact expression can be found in Ref. [40].

The phonon Hamiltonian is accordingly diagonalized in a space spanned by states composed of one, two, and three QRPA phonons.

The eigenfunctions have the structure

$$\begin{aligned}\Psi_\nu(JM) = &\sum_i R_i(\nu J)Q^\dagger_{iJM}|0\rangle \\ &+ \sum_{\substack{i_1\lambda_1\\ i_2\lambda_2}} P^{i_1\lambda_1}_{i_2\lambda_2}(\nu J)[Q^\dagger_{i_1\lambda_1}\otimes Q^\dagger_{i_2\lambda_2}]_{JM}|0\rangle \\ &+ \sum_{\substack{i_1\lambda_1 i_2\lambda_2\\ i_3\lambda_3 I}} T^{i_1\lambda_1 i_2\lambda_2 I}_{i_3\lambda_3}(\nu J) \\ &\times [[Q^\dagger_{i_1\lambda_1}\otimes Q^\dagger_{i_2\lambda_2}]_I\otimes Q^\dagger_{i_3\lambda_3}]_{JM}|0\rangle,\end{aligned} \tag{5}$$

where ν labels the specific QPM excited state of total spin JM.

The above wave functions are properly antisymmetrized according to the procedure outlined in Refs. [28] and [40]. Accounting for the Pauli principle is of special importance for a reliable calculation of the $E2$ and $M1$ transition strengths.

Each transition operator is composed of two pieces [41],

$$M(X\lambda\mu) = M^{(\rm ph)}(X\lambda\mu) + M^{(\rm sc)}(X\lambda\mu). \tag{6}$$

The first term is given by

$$\begin{aligned}M^{(\rm ph)}(X\lambda\mu) = &\frac{1}{2\sqrt{2\lambda+1}} \\ &\times\sum_{ijj'}\langle j\|X\lambda\|j'\rangle(u_jv_{j'}\pm v_ju_{j'}) \\ &\times\left(\psi^{i\lambda}_{jj'}+\varphi^{i\lambda}_{jj'}\right)(Q^\dagger_{i\lambda\mu}+(-)^{\lambda-\mu}Q_{i\lambda-\mu}),\end{aligned} \tag{7}$$

where the $+$ $(-)$ sign holds for time even (odd) operators. The term, being linear in the QRPA phonon operators $Q_{i\lambda\mu}$ and $Q^\dagger_{i\lambda\mu}$, connects states differing by one phonon. This is the leading term and promotes the *Boson allowed* transitions.

The second piece is a quasiparticle scattering term and is given by

$$\begin{aligned}M^{(\rm sc)}(X\lambda\mu) = &\frac{1}{\sqrt{2\lambda+1}} \\ &\times\sum_{ijj'}\langle j\|X\lambda\|j'\rangle(u_ju_{j'}\mp u_ju_{j'}) \\ &\times[\alpha^\dagger_j\times\alpha_{j'}]_{\lambda\mu}\end{aligned} \tag{8}$$

where the $-$ $(+)$ sign holds for time even (odd) operators. This term links only states with the same number of phonons and promotes the *Boson forbidden* transitions. The first term is dominant in the $E2$ transitions. The second is responsible for the $M1$ transitions, which would be forbidden otherwise.

For the numerical calculations, we used the same Woods-Saxon and pairing parameters as in Ref. [38] for the $N = 80$ isotones. Only the quadrupole-quadrupole strength was adjusted so as to get a reasonable fit of the energy and $E2$ strength of the lowest 2^+ state.

TABLE I. Energies and $E2$ decay strengths of the lowest $[2^+]_{\rm RPA}$ states in ^{142}Ce and ^{144}Nd. The corresponding data for ^{138}Ce are also reported for comparison.

Nucleus	λ^π_i	$\omega_{\lambda^\pi_i}$(MeV)	$B(E2)\downarrow$ (W.u.)	% EWSR
^{142}Ce	2^+_1	1.02	19	3.8
	2^+_2	2.13	3	1.24
	2^+_3	2.72	0.03	0.02
^{144}Nd	2^+_1	0.999	19	3.7
	2^+_2	2.08	3.3	1.32
	2^+_3	2.77	0.02	0.01
^{138}Ce	2^+_1	1.02	22.2	4.4
	2^+_2	2.21	1.6	0.7
	2^+_3	2.31	3.96	1.7

III. RESULTS AND DISCUSSION

In both ^{142}Ce and ^{144}Nd, the QRPA yields two low-lying collective 2^+ states (Table I). The lowest one is np symmetric, whereas the second has mixed symmetry. As shown in Table II, in fact, the proton and neutron components are in phase in the first 2^+ state and out of phase in the second. Tables I and II show also that, at an appreciably higher energy, there is a third 2^+ state that is noncollective and describes a proton excitation.

This scheme deviates appreciably from the one obtained for ^{138}Ce [38], shown also here for the sake of clarity. In this nucleus, in addition to the lowest collective isoscalar 2^+ mode, the QRPA yields two 2^+ states, very close in energy, both of dominant MS character and fairly collective, especially the third 2^+.

As pointed out in Ref. [38], the peculiar QRPA 2^+ spectrum in ^{138}Ce is associated with the filling of the proton $g_{7/2}$ subshell and the diffuse Fermi surface induced by pairing.

A question arises naturally at this stage. Why is a much larger $M1$ splitting observed in ^{142}Ce than in ^{138}Ce, having the same number of protons? Why does a large splitting exist

TABLE II. Quasiparticle composition of the lowest $[2^+]_{\mathrm{RPA}}$ states in ^{142}Ce and ^{144}Nd. Only the largest components are given. The states are normalized according to Eq. (2). The data on ^{138}Ce are also reported here for comparison.

Nucleus	State	$(q_1q_2)_n$		$(q_1q_2)_p$	
^{142}Ce	2_1^+	$+0.86(2f_{7/2}\otimes 2f_{7/2})_n$	35%	$+0.51(1g_{7/2}\otimes 1g_{7/2})_p$	12.6%
		$+0.24(2f_{7/2}\otimes 3p_{3/2})_n$	5.3%	$+0.44(2d_{5/2}\otimes 2d_{5/2})_p$	9.0%
		$+0.24(1i_{13/2}\otimes 1i_{13/2})_n$	2.6%	$+0.35(1h_{11/2}\otimes 1h_{11/2})_p$	5.6%
				$+0.24(1g_{7/2}\otimes 2d_{3/2})_p$	4.9%
		Total	54%	Total	46%
	2_2^+	$-1.0(2f_{7/2}\otimes 2f_{7/2})_n$	54%	$+0.65(1g_{7/2}\otimes 1g_{7/2})_p$	21.4%
		$0.1(1h_{11/2}\otimes 2f_{7/2})_n$	0.4%	$+0.47(2d_{5/2}\otimes 2d_{5/2})_p$	11.1%
		Total	55%	Total	45%
	2_3^+	$-0.1(2f_{7/2}\otimes 2f_{7/2})_n$	0.4%	$-0.98(1g_{7/2}\otimes 1g_{7/2})_p$	48.1%
				$0.6(2d_{5/2}\otimes 2d_{5/2})_p$	17.6%
				$-0.57(1g_{7/2}\otimes 2d_{5/2})_p$	32.25%
		Total	1%	Total	99%
^{144}Nd	2_1^+	$+0.88(2f_{7/2}\otimes 2f_{7/2})_n$	37%	$+0.41(1g_{7/2}\otimes 1g_{7/2})_p$	8.1%
		$+0.23(2f_{7/2}\otimes 3p_{3/2})_n$	4.6%	$+0.47(2d_{5/2}\otimes 2d_{5/2})_p$	10.3%
		$+0.2(1i_{13/2}\otimes 1i_{13/2})_n$	2.06%	$+0.42(1h_{11/2}\otimes 1h_{11/2})_p$	8.13%
				$+0.21(1g_{7/2}\otimes 2d_{3/2})_p$	5.3%
		Total	52%	Total	48%
	2_2^+	$-1.1(2f_{7/2}\otimes 2f_{7/2})_n$	56%	$+0.46(1g_{7/2}\otimes 1g_{7/2})_p$	10.3%
		$0.1(1h_{11/2}\otimes 2f_{7/2})_n$	0.6%	$+0.57(2d_{5/2}\otimes 2d_{5/2})_p$	16.2%
		Total	57%	Total	43%
	2_3^+	$-0.1(2f_{7/2}\otimes 2f_{7/2})_n$	0.1%	$0.63(1g_{7/2}\otimes 1g_{7/2})_p$	19.7%
				$-0.95(2d_{5/2}\otimes 2d_{5/2})_p$	45.5%
				$-0.59(1g_{7/2}\otimes 2d_{5/2})_p$	34.4%
		Total	0.2%	Total	99.8%
^{138}Ce	2_1^+	$+0.92(1h_{11/2}\otimes 1h_{11/2})_n$	40.5%	$+0.43(1g_{7/2}\otimes 1g_{7/2})_p$	8.6%
		$+0.46(2d_{3/2}\otimes 2d_{3/2})_n$	10.51%	$+0.31(2d_{5/2}\otimes 2d_{5/2})_p$	4.21%
		$+0.302(2d_{3/2}\otimes 3s_{1/2})_n$	8.9%	$+0.28(1h_{11/2}\otimes 1h_{11/2})_p$	3.43%
				$+0.21(1g_{7/2}\otimes 2d_{3/2})_p$	3.40%
		Total	72%	Total	28%
	2_2^+	$+0.16(1h_{11/2}\otimes 1h_{11/2})_n$	1.15%	$+0.44(1g_{7/2}\otimes 1g_{7/2})_p$	9.84%
		$-1.29(2d_{3/2}\otimes 2d_{3/2})_n$	83.0%	$+0.2(2d_{5/2}\otimes 2d_{5/2})_p$	1.99%
		Total	85%	Total	15%
	2_3^+	$+0.85(1h_{11/2}\otimes 1h_{11/2})_n$	35.92%	$-0.88(1g_{7/2}\otimes 1g_{7/2})_p$	38.9%
		$-0.33(2d_{3/2}\otimes 2d_{3/2})_n$	5.45%	$-0.34(2d_{5/2}\otimes 2d_{5/2})_p$	5.9%
		$+0.18(2d_{3/2}\otimes 3s_{1/2})_n$	3.05%	$-0.23(1h_{11/2}\otimes 1h_{11/2})_p$	2.54%
				$+0.15(1g_{7/2}\otimes 2d_{5/2})_p$	2.23%
		Total	46%	Total	54%

TABLE III. QPM versus experimental [36,37] strengths (in W.u.) of $E2$ and $M1$ transitions in ^{142}Ce and ^{144}Nd.

Nucleus	$J_i \to J_f$	$B(E2)$		$B(M1)$	
		EXP	QPM	EXP	QPM
^{142}Ce	$2_1^+ \to 0_{gs}^+$	$21.2^{+0.24}_{-0.19}$	20		
	$2_2^+ \to 0_{gs}^+$	>0.023	0.20		
	$2_3^+ \to 0_{gs}^+$	$2.5^{+0.2}_{-0.2}$	8.3		
	$2_4^+ \to 0_{gs}^+$	$2.6^{+0.4}_{-0.3}$	0.08		
	$2_5^+ \to 0_{gs}^+$	$0.27^{+0.16}_{-0.15}$	0.15		
	$2_2^+ \to 2_1^+$	>19	23	>0.012	0.004
	$2_3^+ \to 2_1^+$	$2.6^{+0.3}_{-0.3}$	14	$0.13^{+0.01}_{-0.01}$	0.16
	$2_4^+ \to 2_1^+$	$0.037^{+0.006}_{-0.005}$	0.58	$0.20^{+0.03}_{-0.03}$	0.08
	$2_5^+ \to 2_1^+$	$0.028^{+0.017}_{-0.015}$	0.05	$0.0046^{+0.0028}_{-0.0025}$	0.017
^{144}Nd	$2_1^+ \to 0_{gs}^+$	17(1)	15		
	$2_2^+ \to 0_{gs}^+$	0.22(2)	0.005		
	$2_3^+ \to 0_{gs}^+$	$1.7^{+0.4}_{-0.3}$	6.4		
	$2_4^+ \to 0_{gs}^+$	$0.70^{+0.26}_{-0.20}$	0.009		
	$2_5^+ \to 0_{gs}^+$	1.6(3)	0.03		
	$2_6^+ \to 0_{gs}^+$	0.017(7)	0.003		
	$2_2^+ \to 2_1^+$	20(2)	20	$0.03^{+0.03}_{-0.02}$	0.02
	$2_3^+ \to 2_1^+$	$9.4^{+0.2}_{-0.18}$	16	$0.079^{+0.017}_{-0.015}$	0.16
	$2_4^+ \to 2_1^+$	$0.35^{+0.13}_{-0.10}$	1.1	$0.10^{+0.04}_{-0.03}$	0.083
	$2_5^+ \to 2_1^+$	$1.4^{+0.3}_{-0.2}$	0.14	$0.02^{+0.004}_{-0.003}$	0.013
	$2_6^+ \to 2_1^+$	$0.26^{+0.11}_{-0.10}$	0.26	$0.012^{+0.005}_{-0.005}$	0.009

also in ^{144}Nd, with two valence protons in excess with respect to the $g_{7/2}$ subshell closure, but is absent in ^{136}Ba, with two proton holes with respect to the closure of the same subshell? We try to give an answer to these questions by going from the QRPA to the QPM.

A few QPM observables are compared with the experimental data in Table III and in Figs. 1 and 2. As shown pictorially in Fig. 1, the strength distributions of the $E2$ transitions to the ground and 2_1^+ states are quite similar in ^{142}Ce and ^{144}Nd. Concerning the $E2$ transitions to the ground state, most of the strength is concentrated into the lowest 2_1^+ state of each nucleus at 0.641 and 0.696 MeV, respectively. The remaining $E2$ strength, about 5.4 and 4.2 W.u., respectively, is distributed mainly among two or three 2^+ states in the energy range 2–2.6 MeV. The calculation reproduces the lowest prominent peak, but overestimates the remaining strength by a factor of 1.5 and does not account for its fragmentation. An agreement of the same quality is obtained for the $E2$ transitions to the first 2_1^+ (Fig. 1). The QPM overestimates the second peak at the expense of the fragmentation.

As already pointed out in the Introduction, the large splitting of the $M1$ strength represents the main feature of the low-lying spectra in ^{142}Ce and ^{144}Nd. We observe, in fact, two main peaks, of comparable height, separated by 364 keV in ^{142}Ce and by about 200 keV in ^{144}Nd (Fig. 2). They correspond to the transitions to the 2_1^+ state from the 2_3^+ and 2_4^+ states (Table III).

The QPM yields also a similar result, though the splitting is somewhat larger. Other discrepancies may be noticed. The QPM underestimates the second large peak in ^{142}Ce and overestimates the lowest large peak in ^{144}Nd. The overall strength is comparable with experiments in both nuclei. It is remarkable, in any case, that the calculation accounts for the main properties of the spectra. We feel, therefore, entitled to try to find within the QPM scheme the reason for such a pronounced $M1$ splitting in ^{142}Ce and ^{144}Nd. We resort to the QPM also in an attempt to explain why such a splitting is noticeable only in ^{138}Ce and is absent in ^{134}Xe and ^{136}Ba.

As shown in Table IV, in both nuclei ^{142}Ce and ^{144}Nd the lowest QRPA isoscalar quadrupole state is the dominant component of the first QPM 2_1^+ state. This state also has an appreciable two-phonon component. In both nuclei, the second, third, and fourth QPM 2^+ states are linear combinations of one- and two-phonon configurations. A three-phonon component is also present with a large amplitude in the third and

TABLE IV. Energy and phonon structure of selected low-lying excited states. Only the dominant components are presented.

Nucleus	State J^π	E (keV)		Phonon structure (%)
		EXP	QPM	
^{142}Ce	2_1^+	641	485	$72\%[2_1^+]_{RPA} + 12\%[2_1^+ \otimes 2_1^+]_{RPA}$
	2_2^+	1536	1588	$49\%[2_1^+ \otimes 2_1^+]_{RPA} + 9\%[2_1^+]_{RPA} + 31\%[2_2^+]_{RPA}$
	2_3^+	2004	2070	$50\%[2_2^+]_{RPA} + 11\%[2_1^+]_{RPA} + 9\%[2_1^+ \otimes 2_1^+]_{RPA} + 17\%[2_1^+ \otimes 2_1^+ \otimes 2_1^+]_{RPA}$
	2_4^+	2364	2603	$13\%[2_2^+]_{RPA} + 12\%[2_1^+ \otimes 2_1^+]_{RPA} + 16\%[2_1^+ \otimes 2_2^+]_{RPA} + 28\%[2_1^+ \otimes 2_1^+ \otimes 2_1^+]_{RPA}$
	2_5^+	2543	2611	$87\%[2_3^+]_{RPA}$
^{144}Nd	2_1^+	696	520	$75\%[2_1^+]_{RPA} + 8\%[2_1^+ \otimes 2_1^+]_{RPA}$
	2_2^+	1560	1655	$49\%[2_1^+ \otimes 2_1^+]_{RPA} + 6\%[2_1^+]_{RPA} + 36\%[2_2^+]_{RPA}$
	2_3^+	2073	2130	$43\%[2_2^+]_{RPA} + 10\%[2_1^+]_{RPA} + 14\%[2_1^+ \otimes 2_1^+]_{RPA} + 18\%[2_1^+ \otimes 2_1^+ \otimes 2_1^+]_{RPA}$
	2_4^+	2269	2618	$15\%[2_2^+]_{RPA} + 15\%[2_1^+ \otimes 2_1^+]_{RPA} + 14\%[2_1^+ \otimes 2_2^+]_{RPA} + 30\%[2_1^+ \otimes 2_1^+ \otimes 2_1^+]_{RPA}$
	2_5^+	2528	2755	$68\%[2_3^+]_{RPA} + 11\%[2_4^+]_{RPA}$
	2_6^+	2592	2790	$24\%[2_3^+]_{RPA} + 67\%[2_4^+]_{RPA}$

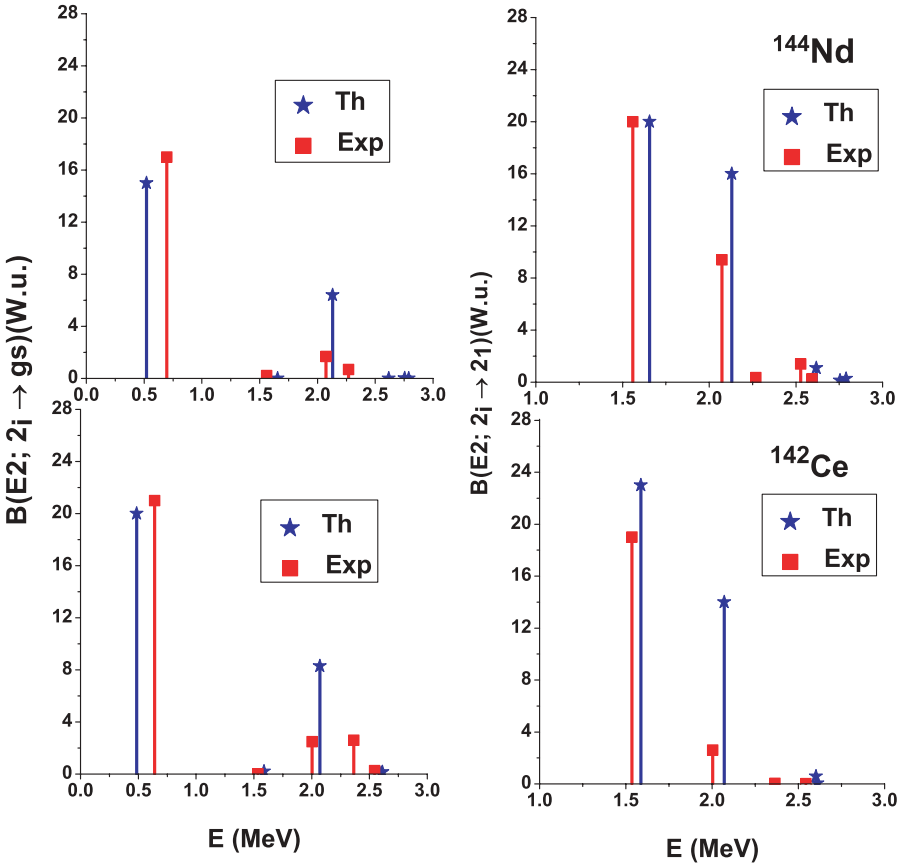

FIG. 1. (Color online) Experimental [36,37] and QPM strength distributions of the $2_i^+ \to 0_{gs}^+$ and $2_i^+ \to 2_1^+$ $E2$ transitions in ^{142}Ce and ^{144}Nd.

forth states. In the second 2_2^+ state the quadrupole-quadrupole two-phonon state $[2_1^+ \otimes 2_1^+]_{\rm RPA}$ is prominent, while the MS one-phonon $[2_2^+]_{\rm RPA}$ component is prevalent in the third 2_3^+ state. The fourth 2_4^+ state has an even more composite structure with one-, two-, and, even three-phonon components, all of comparable amplitude.

The immediate reason for the $M1$ splitting is to be found in the mentioned composite phonon structure of the QPM states. From Tables III and IV one infers that the first prominent peak is due to the collective MS $[2_2^+]_{\rm RPA}$ component present with large amplitude in the 2_3^+ state. The second arises from the combined presence in the fourth 2_4^+ state of the same one-phonon MS $[2_2^+]_{\rm RPA}$ plus the two-phonon MS component $[2_1^+ \otimes 2_2^+]_{\rm RPA}$. The two components are respectively coupled by the $M1$ operator to the symmetric one-phonon $[2_1^+]_{\rm RPA}$ and $[2_1^+ \otimes 2_1^+]_{\rm RPA}$, the two main components of the isoscalar QPM 2_1^+ state.

The phonon fragmentation of the QPM 2^+ states is determined mostly by the squared matrix elements of the coupling term H_{vq} between one-and two-phonon states versus the energy difference between the same one- and two-phonon components. The coupling term depends on the shell structure and increases with the collectivity of the RPA phonons involved.

The one- to two-phonon matrix elements of the coupling Hamiltonian are comparable in the $N = 80$ isotone ^{138}Ce and the $N = 84$ isotones ^{142}Ce and ^{144}Nd. From looking at Table I, however, one can see that in ^{142}Ce the energy of the second RPA $[2_2^+]_{\rm RPA}$ is almost twice the energy of the lowest RPA quadrupole phonon. This small energy difference between the MS one-phonon and the symmetric two-phonon components, in both nuclei ^{142}Ce and ^{144}Nd, enhances considerably the coupling between these configurations and, therefore, their admixture in the QPM states leading finally to the fragmentation of the $M1$ strength. In ^{138}Ce, instead, the energy difference is slightly larger. Moreover, the collectivity is shared among the second and third RPA phonons $[2_2^+]_{\rm RPA}$ and $[2_3^+]_{\rm RPA}$, very close in energy and, therefore, strongly interacting. This mitigates their coupling with the two-phonon configuration $[2_1^+ \times 2_1^+]_{\rm RPA}$.

TABLE V. Energy of the lowest two-quasiparticle neutron and proton states in ^{142}Ce and ^{138}Ce. The proton states are the same for both isotopes.

	$q_1 q_2$	$E_{q_1} + E_{q_2}$ (MeV)
$N = 80$	$(2d_{3/2} \otimes 2d_{3/2})_n$	2.191
	$(2h_{11/2} \otimes 1h_{11/2})_n$	2.491
	$(2d_{3/2} \otimes 3s_{1/2})_n$	2.648
$N = 84$	$(2f_{7/2} \otimes 2f_{7/2})_n$	1.984
	$(2f_{7/2} \otimes 1h_{9/2})_n$	3.422
	$(2f_{7/2} \otimes 3p_{3/2})_n$	3.831
$Z = 58$	$(1g_{7/2} \otimes 1g_{7/2})_p$	2.627
	$(1g_{7/2} \otimes 2d_{5/2})_p$	2.892
	$(2d_{5/2} \otimes 2d_{5/2})_p$	3.158

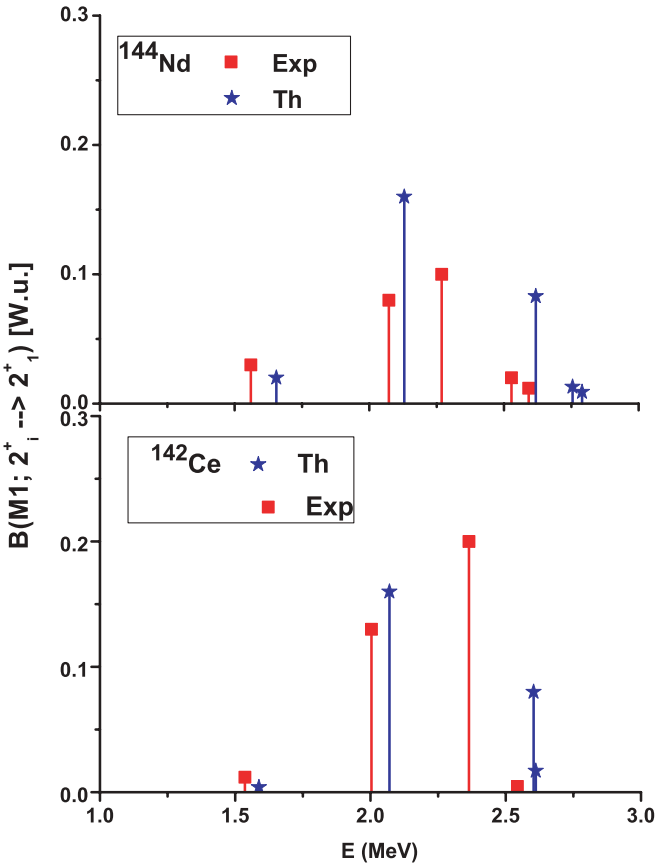

FIG. 2. (Color online) QPM versus experimental [36,37] strength distributions of the $2_i^+ \rightarrow 2_1^+$ $M1$ transitions in ^{142}Ce and ^{144}Nd.

To complete the picture, we add that in ^{136}Ba the energy difference between the MS one-phonon and the symmetric two-phonon states is small, as for the $N = 84$ isotones, but the one- to two-phonon coupling term is considerably smaller than that in the $N = 84$ isotones because the isovector $[2_2^+]_{\rm RPA}$ phonon is less collective. As shown in Table I of Ref. [38], it exhausts 0.71% of the energy-weighted sum rule (EWSR), almost a factor of 2 less than in the case of the $N = 84$ isotones (Table I).

The effectiveness of the phonon coupling in inducing pronounced phonon admixtures in the QPM states of the $N = 84$ isotones is not accidental but is due to their specific neutron shell structure. Let us compare the WS single-particle spectra in ^{138}Ce and ^{142}Ce. The proton spectra are the same, of course. The neutron single-particle levels in ^{138}Ce are closely packed. In ^{142}Ce, instead, we have a gap between the $2f_{7/2}$ shell and the other levels all close in energy. This difference yields an asymmetry between the two-quasiparticle and two-quasihole neutron spectra. As shown in Table V, while the lowest three two-quasihole levels are close and almost equidistant, a large gap exists between the lowest two-quasiparticle level and the other two. The different strength fragmentations in $N = 80$ and $N = 84$ isotones, respectively, are ultimately to be ascribed to the asymmetry between particle and hole spectra with respect to the closed shell $N = 82$.

IV. CONCLUDING REMARKS

The pronounced splitting observed in the $N = 84$ isotones for the strength of the $M1$ transitions, coupling the MS to the symmetric 2^+ states, is an effect of the fragmentation of the RPA collective MS quadrupole phonon among two QPM 2^+ states. The fragmentation is the result of the phonon coupling which, in the $N = 84$ nuclei explored here, is especially effective because of the quasidegeneracy of the MS RPA 2^+ state with the symmetric quadrupole-quadrupole two-phonon states.

Such a degeneracy is due to the gap between j subshells present in the neutron single-particle spectrum above the $N = 82$ closed shell. The gap is absent in the neutron-hole spectra of the $N = 80$ isotones. Hence, the lack of splitting in nuclei like ^{136}Ba.

A small splitting was observed also in ^{138}Ce. In this nucleus, the mechanism responsible for such a phenomenon was a different one. It was promoted by the gap in correspondence of the proton $1g_{7/2}$ subshell closure and the pairing responsible for the diffuseness of the Fermi surface, which yields a relatively higher density of two-quasiparticle states at low energy. Though different, both mixing mechanisms are genuine shell effects that can be explained only within a microscopic context that goes beyond QRPA.

Serious discrepancies between the QPM calculations and the experiments have been pointed out. These differences could be partially cured by acting on the QPM parameters. It is remarkable that, by using the same parameters, we obtain substantially different responses in particle-hole conjugate nuclei. This makes us confident about the reliability of our analysis.

For a conclusive response, it would be desirable to perform new experiments that would produce more data on the $N = 84$ isotones, e.g., on the neutron-rich isotone ^{140}Ba. Moreover, it would be extremely important to investigate experimentally the $N = 80$ isotones, e.g., the isotone ^{140}Nd. Being the neutron-hole conjugate of ^{144}Nd, this nucleus would provide a stringent test of our theoretical interpretation.

ACKNOWLEDGMENTS

One of the authors (Ch.S.) acknowledges financial support within the agreement between the INFN and the Bulgarian Science Foundation. Two of us (N.P. and Ch.S.) acknowledge financial support under the DAAD-08 German and DAAD-09 Bulgarian contracts.

[1] F. Iachello and A. Arima, *The Interacting Boson Model* (Cambridge University Press, Cambridge, UK, 1987).
[2] A. Arima, T. Otsuka, F. Iachello, and I. Talmi, Phys. Lett. **B66**, 205 (1977).
[3] T. Otsuka, A. Arima, and F. Iachello, Nucl. Phys. **A309**, 1 (1978).
[4] F. Iachello, Phys. Rev. Lett. **53**, 1427 (1984).
[5] N. Lo Iudice and F. Palumbo, Phys. Rev. Lett. **41**, 1532 (1978).

[6] D. Bohle, A. Richter, W. Steffen, A. E. L. Dieperink, N. Lo Iudice, F. Palumbo, and O. Scholten, Phys. Lett. **B137**, 27 (1984).
[7] A. Richter, Prog. Part. Nucl. Phys. **34**, 261 (1995).
[8] U. Kneissl, H. H. Pitz, and A. Zilges, Prog. Part. Nucl. Phys. **37**, 349 (1996).
[9] N. Lo Iudice, Riv. Nuovo Cimento **23**(9), 1 (2000).
[10] K. P. Lieb, H. G. Börner, M. S. Dewey, J. Jolie, S. J. Robinson, S. Ulbig, and Ch. Winter, Phys. Lett. **B215**, 50 (1988).
[11] H. Nakada, T. Otsuka, and T. Sebe, Phys. Rev. Lett. **67**, 1086 (1991).
[12] N. Pietralla, C. Fransen, D. Belic, P. von Brentano, C. Friessner, U. Kneissl, A. Linnemann, A. Nord, H. H. Pitz, T. Otsuka, I. Schneider, V. Werner, and I. Wiedenhover, Phys. Rev. Lett. **83**, 1303 (1999).
[13] N. Pietralla, C. Fransen, P. von Brentano, A. Dewald, A. Fitzler, C. Friessner, and J. Gableske, Phys. Rev. Lett. **84**, 3775 (2000).
[14] C. Fransen, N. Pietralla, P. von Brentano, A. Dewald, J. Gableske, A. Gade, A. F. Lisetskiy, and V. Werner, Phys. Lett. **B508**, 219 (2001).
[15] C. Fransen, N. Pietralla, Z. Ammar, D. Bandyopadhyay, N. Boukharouba, P. von Brentano, A. Dewald, J. Gableske, A. Gade, J. Jolie, U. Kneissl, S. R. Lesher, A. F. Lisetskiy, M. T. McEllistrem, M. Merrick, H. H. Pitz, N. Warr, V. Werner, and S. W. Yates, Phys. Rev. C **67**, 024307 (2003).
[16] O. Burda, N. Botha, J. Carter, R. W. Fearick, S. V. Förtsch, C. Fransen, H. Fujita, J. D. Holt, M. Kuhar, A. Lenhardt, P. von Neumann-Cosel, R. Neveling, N. Pietralla, V. Yu. Ponomarev, A. Richter, O. Scholten, E. Sideras-Haddad, F. D. Smit, and J. Wambach, Phys. Rev. Lett. **99**, 092503 (2007).
[17] N. Pietralla, C. J. Barton, R. Krücken, C. W. Beausang, M. A. Caprio, R. F. Casten, J. R. Cooper, A. A. Hecht, H. Newman, J. R. Novak, and N. V. Zamfir, Phys. Rev. C **64**, 031301(R) (2001).
[18] V. Werner, D. Belic, P. von Brentano, C. Fransen, A. Gade, H. von Garrel, J. Jolie, U. Kneissl, C. Kostall, A. Linnemann, A. F. Lisetskiy, N. Pietralla, H. H. Pitz, M. Scheck, K.-H. Speidel, F. Stedile, and S. W. Yates, Phys. Lett. **B550**, 140 (2002).
[19] C. Fransen, N. Pietralla, A. P. Tonchev, M. W. Ahmed, J. Chen, G. Feldman, U. Kneissl, J. Li, V. Litvinenko, B. Perdue, I. V. Pinayev, H.-H. Pitz, R. Prior, K. Sabourov, M. Spraker, W. Tornow, H. R. Weller, V. Werner, Y. K. Wu, and S. W. Yates, Phys. Rev. C **70**, 044317 (2004).
[20] C. Fransen, V. Werner, D. Bandyopadhyay, N. Boukharouba, S. R. Lesher, M. T. McEllistrem, J. Jolie, N. Pietralla, P. von Brentano, and S. W. Yates, Phys. Rev. C **71**, 054304 (2005).
[21] E. Elhami, J. N. Orce, S. Mukhopadhyay, S. N. Choudry, M. Scheck, M. T. McEllistrem, and S. W. Yates, Phys. Rev. C **75**, 011301(R) (2007).
[22] S. R. Lesher, C. J. McKay, M. Mynk, D. Bandyopadhyay, N. Boukharouba, C. Fransen, J. N. Orce, M. T. McEllistrem, and S. W. Yates, Phys. Rev. C **75**, 034318 (2007).
[23] D. Bandyopadhyay, S. R. Lesher, C. Fransen, N. Boukharouba, P. E. Garrett, K. L. Green, M. T. McEllistrem, and S. W. Yates, Phys. Rev. C **76**, 054308 (2007).
[24] N. Pietralla, C. Fransen, A. Gade, N. A. Smirnova, P. von Brentano, V. Werner, and S. W. Yates, Phys. Rev. C **68**, 031305(R) (2003).
[25] H. Klein, A. F. Lisetskiy, N. Pietralla, C. Fransen, A. Gade, and P. von Brentano, Phys. Rev. C **65**, 044315 (2002).
[26] N. Pietralla, P. von Brentano, and A. F. Lisetskiy, Prog. Part. Nucl. Phys. **60**, 225 (2008).
[27] N. Lo Iudice and Ch. Stoyanov, Phys. Rev. C **62**, 047302 (2000).
[28] N. Lo Iudice and Ch. Stoyanov, Phys. Rev. C **65**, 064304 (2002).
[29] N. Lo Iudice and Ch. Stoyanov, Phys. Rev. C **69**, 044312 (2004).
[30] N. Lo Iudice and Ch. Stoyanov, Phys. Rev. C **73**, 037305 (2006).
[31] A. F. Lisetskiy, N. Pietralla, C. Fransen, R. V. Jolos, and P. von Brentano, Nucl. Phys. **A677**, 100 (2000).
[32] N. Boelaert, N. Smirnova, K. Heyde, and J. Jolie, Phys. Rev. C **75**, 014316 (2007).
[33] N. Pietralla, D. Belic, P. von Brentano, C. Fransen, R.-D. Herzberg, U. Kneissl, H. Maser, P. Matschinsky, A. Nord, T. Otsuka, H. H. Pitz, V. Werner, and I. Wiedenhover, Phys. Rev. C **58**, 796 (1998).
[34] G. Rainovski, N. Pietralla, T. Ahn, C. J. Lister, R. V. F. Janssens, M. P. Carpenter, S. Zhu, and C. J. Barton III, Phys. Rev. Lett. **96**, 122501 (2006).
[35] T. Ahn, N. Pietralla, G. Rainovski, A. Costin, K. Dusling, T. C. Li, A. Linnemann, and S. Pontillo, Phys. Rev. C **75**, 014313 (2007).
[36] J. R. Vanhoy, J. M. Anthony, B. M. Haas, B. H. Benedict, B. T. Meehan, S. F. Hicks, C. M. Davoren, and C. L. Lundstedt, Phys. Rev. C **52**, 2387 (1995).
[37] S. F. Hicks, C. M. Davoren, W. M. Faulkner, and J. R. Vanhoy, Phys. Rev. C **57**, 2264 (1998).
[38] N. Lo Iudice, Ch. Stoyanov, and D. Tarpanov, Phys. Rev. C **77**, 044310 (2008).
[39] Thai Khac Dinh, M. Grinberg, and Ch. Stoyanov, J. Phys. G: Nucl. Part. Phys. **18**, 329 (1992).
[40] V. G. Soloviev, *Theory of Atomic Nuclei: Quasiparticles and Phonons* (Institute of Physics Publishing, Bristol, 1992).
[41] V. Yu. Ponomarev, Ch. Stoyanov, N. Tsoneva, and M. Grinberg, Nucl. Phys. **A635**, 470 (1998).